International Journal of Nanomaterials and Chemistry

http://dx.doi.org/10.18576/ijnc/030202

Influence of Fe-doping on the Stress Behaviour in ZnO thin Films Synthesized by Electrochemical Method

K. Al-heuseen[*] *and M. Kh. Alquran*

Ajloun University College, Al-Balqa Applied University, Jordan.

Received: 2 Feb. 2017, Revised: 22 Apr. 2017, Accepted. 28 Apr. 2017.
Published online: 1 May 2017.

Abstract: Fe-doped ZnO nanostructured thin films were deposited on gold-coated glass substrates, using electrochemical deposition technique at room temperature for different concentrations of Fe. Structural and optical characterizations were carried out using various techniques, to investigate the properties of the samples. The influence of iron doping on the structural, morphological, stress and optical properties of the films was studied. From the XRD pattern, it is observed that peak positions shift towards lower angles with Fe doping. The change in the peak positions with increase in Fe content clearly indicates that Fe ions replace Zn ions in the ZnO films. XRD patterns and Raman analysis showed that ZnO films suffered a compressive stress for undoped ZnO and changed to tensile stress with increase in the Fe concentration. The growth and doping mechanism was also briefly discussed.

Keywords: Fe-doped ZnO; Doping; Electrochemical deposition; Stress.

1 Introduction

The interest in ZnO is due to its unique properties, such as a relatively high exciton binding energy (60 MeV), wide direct band gap (3.37 eV at 300 K), piezoelectric behavior, and the fact that it is a biocompatible material [1]. ZnO has a broad range of applications such as light-emitting diodes, photo detectors, and gas sensors [2,4].

The undoped and doped ZnO can be fabricated using various methods, such as radio frequency plasma [5], ion-assisted cyclic sputtering [6], RF sputtering [7], thermal oxidation [8], electron beam evaporation [9], activated reactive evaporation [10], spray pyrolysis [11], low-pressure metal organic chemical vapor deposition (MOCVD) [12], chemical bath deposition [13], and electrodeposition [14]. Compared to other techniques, electrochemical methods offer several advantages including fast, simple, low cost, operate at near room temperature, large-scale deposition area, and its ability to control composition, crystallinity and the properties of the deposit by adjusting deposition conditions. Moreover, the deposition process can be carried out on various substrates such as glass, polymers, semiconductors, and templates. There are no special requirements needed for the substrates, except that it should be conductive. Therefore, this technique is well adapted for industrial procedures in the fabrication of ZnO thin films.

However, several inconsistent results have been obtained for the Fe-doped ZnO films. Polyakov et al. [15] found room temperature ferromagnetism by implanting Fe ions in a ZnO crystal grown by vapour phase while, Janisch et al. [16] reported that Fe-doped ZnO showed a paramagnetic behaviour. In order to clarify this discrepancy, it is important to disclose the effect of doped-Fe on the structure and properties of ZnO thin films. For the Fe-doped ZnO materials, the results of some theoretical studies show that they can possess ferromagnetic properties at room temperature [17, 18]; therefore, most of the researchers mainly studied the ferromagnetic behaviour of Fe-doped ZnO thin films [19,21]. There are few reports on their structural, optical and electrical properties. However, Fe-doped ZnO thin film could be an important multi-functional material; hence, it is important to study its structural, optical and electrical properties and the correlation between them. The growth stress, which results into defects in the thin film, is due to the unbalanced stoichiometry between Zn and O in ZnO crystals. In other words, the intrinsic stress in ZnO could be controlled by adjusting the growth parameters.

The present paper describes the process of controlling stress in Fe-doped ZnO nanostructures via Fe concentrations at room temperature by electrochemical techniques on gold coated glass substrates in an aqueous solution.

The objective of the current trial is, first, to show how stress in Fe-doped ZnO nanostructures could be converted from compressive in undoped to tensile in doped, by controlling the Fe concentrations during the electrochemical deposition process. Second, the present

[*] Corresponding author E-mail: kalhussen@yahoo.com

© 2017 NSP
Natural Sciences Publishing Cor.

study demonstrates the correlation between the stress state of ZnO films and variation in the lattice constant.

2 Experimental Procedure

Fe doped ZnO nanostructures were deposited by Electrochemical deposition (ECD) using 0.1 M Zn $(NO_3)_2$ aqueous solutions and a stock solution of 4.13 mM Fe $(NO_3)_3$ were dissolved in deioniezed water. To adjust the composition of the deposits, the concentration of Fe $(NO_3)_3$ in the baths were 10 µl, 20 µl, 30 µl, and 40 µl. These correspond to the concentrations of Fe ions in the bath of 0.06 mM, 0.12 mM, 0.18 mM, and 0.24 mM respectively.

A simple two-electrode homemade Teflon cell was constructed using a platinum wire as an anode and the gold coated glass substrate as a cathode. The gold coating is sufficiently thin such that it does allow transmittance measurements unhindered. The thicknesses of gold layers were about 20 nm. The distance between the anode and the substrate was about 0.5 cm. A constant electrodeposition current density of 3 mA/cm^2 produces the highest deposition rate was applied for 30 min. The good conductor gold layer was used to reduce the stress in the deposited films and to increase the deposition rate.

Finally, the synthesized products were characterized by X-ray diffraction (XRD) and Raman spectroscopy.

3 Results and Discussions

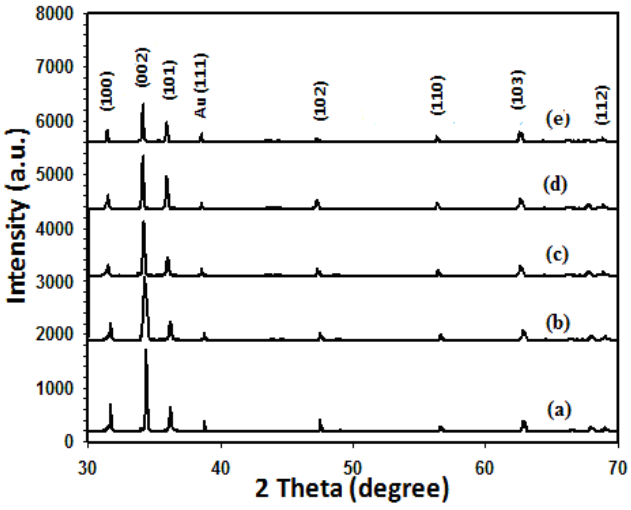

Fig.1: XRD spectra of of (a) pure ZnO, b) 10µl Fe, (c) 20 µl Fe, (d) 30 µl Fe, and (e) 40 µl Fe-doped ZnO thin films.

Fig.1 show the XRD spectra of (a) pure ZnO, (b) 10µl Fe, (c) 20 µl Fe, (d) 30 µl Fe, and (e) 40 µl Fe-doped ZnO thin films respectively. In all cases, the observed diffraction peaks can be indexed to standard hexagonal wurtzite ZnO structure, which indicated that Fe-doping did not change the hexagonal wurtzite structure of ZnO films. Seven peaks appear in the diffraction spectrum in the 2θ interval of 30-70°, and correspond to (100), (002), (101), (102), (110), (103) and (112) orientations of the ZnO hexagonal structure. The film formed is polycrystalline with a preferential orientation of the (002) diffraction peak, showing that the film is preferentially oriented along the c-axis direction. This indicates that this axis in the ZnO film tends to grow perpendicular to the substrate surface [22]. In the XRD pattern, characteristic peaks of the (111) gold substrate also appears.

The peaks are shifted to lower angles and the intensity decreased with increasing Fe doping concentration compared to those of pure ZnO, which is consistent with that of other Fe-doped ZnO films [22]. This shift in peak positions clearly reflects that Fe replaces Zn in the ZnO films. Meanwhile, it was apparent that the intensity and the full width at half maximum (FWHM) of (002) diffraction peak decreasing with the increment of Fe concentration, implying that the more the Fe concentration in ZnO films improves the ZnO films crystallinity.

This might be due to the lattice disorder and strain induced by interstitial Fe atoms or the substitution of Fe for Zn. The lattice constant of Fe doped ZnO films were found to be slightly larger than those of pure ZnO. The larger ionic radii of Fe^{+2} ions (0.63 A°) compared to Zn^{+2} ions (0.60 A°) in the tetrahedral coordination [23,24] tends to increase the size of the lattice in doped ZnO films. An approximate average size D of Fe-ZnO crystal was calculated from the well known Scherrer formula:

$$D = \frac{K\lambda}{\beta \cos\theta} \qquad (1)$$

where k is a constant equal to 0.9, λ is the incident x-ray wavelength and β is the FWHM in radian. The values of D and the unit cell volume V for all doped samples are listed in Table 1. They are obviously increased with doping concentrations.

Fig. 2 summarizes the variation of the lattice constants and crystallite size with Fe doping concentrations. The constants *a* and *c* saturated for higher Fe concentrations; meanwhile the crystallite size D increases almost linearly with Fe concentration. The out of plane (along c-axis) strain, ε_c, see Table 1, have been calculated from the relation $\varepsilon_c = \Delta c/c_0$ [25], where; Δc is defined as the deviation of the calculated lattice parameter *c* from the corresponding unstrained values of bulk ZnO. Positive values for ε_c denote tensile strain while negative ones denote compressive strain. The positive values of the out of plane strain $\boldsymbol{\varepsilon_c}$ indicate that the strain caused by the substrate is tensile in all doped samples except for the undoped sample. As the Fe doped concentration of the films increases, the strain increases and affects the values of lattice parameters *a* and *c*.

© 2017 NSP
Natural Sciences Publishing Cor.

Table 1. Lattice constants (c), (a), out of plane strain (ε_c), stress (σ), unit cell volume V and average crystal size D determined for the Fe-ZnO samples deposited for different durations.

Sample	*a* (A°)	c (A°)	ε_c (%)	D (nm)	$V=a^2c\sqrt{3}/2$	σ(GPa)
Pure ZnO	3.36	5. 19	-0.44	66	0.0507	-14.2604
10Fe	3.50	5.224	0.13	74	0.0554	4.213286
20Fe	3.60	5.239	0.52	80	0.0588	16.85315
30Fe	3.64	5.254	0.71	90	0.0602	23.01103
40Fe	3.68	5.254	0.71	94	0.0616	23.01103

Table 2. The phonon modes detected in the Raman spectra.

Sample	E_1(LO)	A_1(TO)	E_1(TO)	E_2(high)	Stress (GPa)	FWHM of E_2(high)(cm^{-1})
Pure ZnO	584.872	384.032	413.340	439.30	0.45	12
10Fe	584.034	383.212	412.125	436.50	-0.098	11
20Fe	583.644	382.144	411.061	435.90	-0.21	11
30Fe	582.578	381.59	410.517	435.50	-0.29	10
40Fe	583.644	379.41	409.429	435.01	-0.39	11

In addition, the strain increases with Fe doping concentrations. Employing the data above, the stress (σ) in the plane of the films was calculated using the strain model for hexagonal crystals Eq. (2) [26,27]

$$\sigma_{film} = \left(\frac{2C_{13}^2 - C_{33}(C_{11} - C_{12})}{C_{13}}\right) * \varepsilon_c \qquad (2)$$

Where (σ) refer to the mean stress in the ZnO film, C_{11} = 209.7 GPa, C_{12} = 121.1 GPa, C_{13} = 105.1 GPa and C_{33} = 210.9 GPa are the elastic stiffness constants of the bulk ZnO and ε_c is the out of plane (along c-axis) strain. The estimated values of stress (σ) in the ZnO films for (0 0 2) plane, grown at different doping concentrations are as listed in Table 1 and Fig.4.

Fig. 3 shows the Raman spectra for the ZnO thin films as a function of Fe doping concentrations. The typical Raman spectrum excited by an argon ion laser (514.5 nm) was used as an excitation source. The Raman scattering spectrum is a sensitive and highly useful method for determining crystal perfection and structural defects. In this study, it was used to clarify the structure of Fe-ZnO nanostructures for different Fe concentrations.

The wurtzite-type ZnO belongs to the space group C^4 (P63mc) with two formula units in the primitive cell. Raman spectra are sensitive to the crystal quality, structural defects, and disorders of the grown products. The E_1 mode is a polar mode and is split into transverse optical (TO) and longitudinal optical (LO) branches [28]. The phonon peak positions for ZnO samples, using different Fe concentrations are summarized in Table2.

As we can see in the spectra, a sharp, strong and dominant E_2(high) mode of Fe-ZnO nanostructures are observed. This result is in good agreement with the XRD and SEM analysis. The intensity of E_2(high) of doped Fe-ZnO is much higher than that of un-doped, which may be caused due to the different degree of crystallization [29]. Two small peaks at 410 and 381.5 cm^{-1} observed in the spectrum are assigned as E_1(TO) and A_1(TO) modes, respectively.

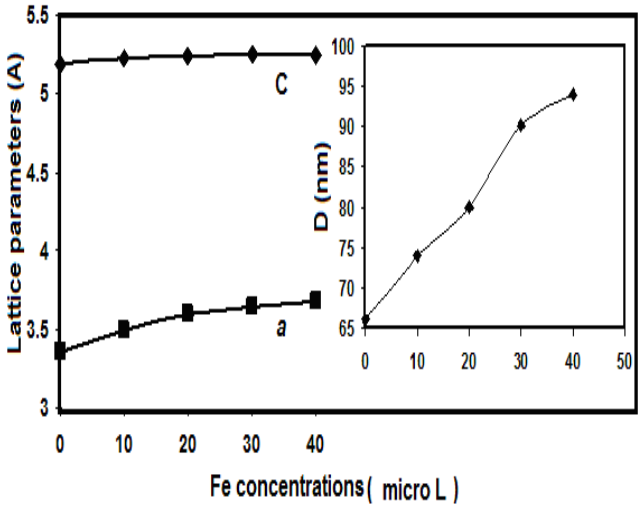

Fig. 2: Variation of lattice constants *a* and *c* and grain size D of Fe-ZnO thin films with Fe concentrations.

Additionally, the peak at 583.6 cm^{-1} is attributed to the E_1(LO) mode, which detected for all the samples, which have been regarded to be associated with the defects of O vacancies, Zn interstitials or their complexes and free carriers [30].

This should be the reason why the defect level induced visible emission band in our ZnO nanostructures PL spectra. In addition, there are another two peaks A_1 at 331 and at 664 cm^{-1} may be from acoustic overtone. In order to investigate the behavior of stress in Fe-ZnO films, it was

shown that the E_2 (high) optical phonon mode of the Fe-ZnO thin films was seen at different positions, shifted up or down when compared with that for the stress-free bulk ZnO, recorded at a value of 437 cm^{-1} [31]. This observation indicated that all the samples had a wurtzite structure and a non-polar mode [32].

© 2017 NSP
Natural Sciences Publishing Cor.

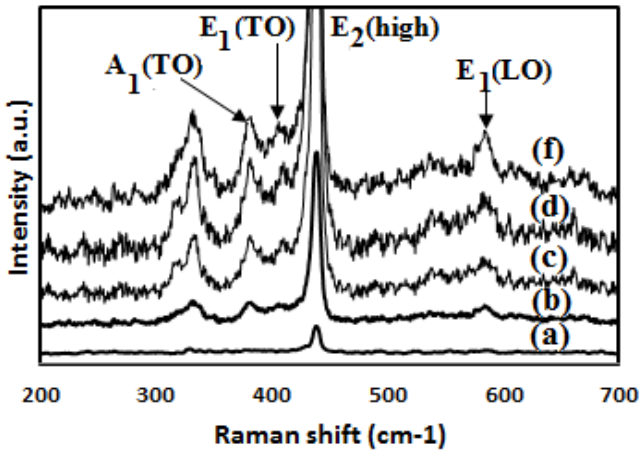

Fig. 3: Raman spectra of (a) pure ZnO, b) 10µl Fe, (c) 20 µl Fe, (d) 30 µl Fe, and (e) 40 µl Fe-doped ZnO thin films.

Since the E_2 mode of ZnO represents a wurtzite structure, its shift could provide information on the stress. Likewise, an increase in the E_2 (high) photon frequency (ω) has been ascribed to the compressive stress, whereas a decrease in the E_2 (high) phonon frequency was ascribed to tensile stress [33].

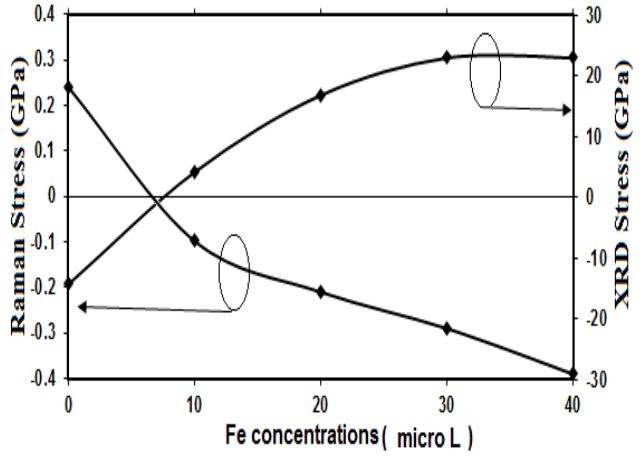

Fig. 4: Variation in stress in the Fe-ZnO thin films with Fe concentrations.

In the un-doped sample (a), the position of the E_2 high shifted up to 438.3 cm^{-1} (2.3 cm^{-1}), indicating that the ZnO film suffered from a compressive stress. On the other hand, in the samples doped for 10, 20,30 and 40 Fe%, the positions of the E_2 high phonon mode were observed at 436.50, 435.90, 435.50 and 435.01 cm^{-1}, respectively, implying a downward shift of about 0.5, 1.1, 1.5 and 1.99 cm^{-1}, respectively. The shift in the position of E_2 high phonon mode downwards indicated that the ZnO films were subjected to increasing tensile stress with increase in Fe concentrations. The calculation of stress of Fe-ZnO thin films was then carried out, taking into account these recorded shifts with increase in pressure (5.1 cm^{-1}/GPa [34]). From this calculation, the compressive and tensile stresses were thus estimated to be 0.45, 0.098, 0.21, 0.29 and 0.39 GPa. These results are well in agreement with that of the XRD analysis.

Finally, the possible electro deposition mechanism of ZnO through nitrate precursors can be summarized as follows:

First, the reduction of nitrate ions produces nitrite and hydroxide ions in water. Then, Zn ions interact with hydroxide ions, forming Zinc Hydroxides. After dehydration of Zn $(NO_3)_2$ the final product ZnO forms [35,36].

$$Zn(NO_3)_2 + H_2O \rightarrow Zn^{2+} + NO_3^{1-} \quad (3)$$

$$NO_3^{1-} + H_2O + 2e^- \rightarrow NO_2^{1-} + 2OH^- \quad (4)$$

$$Zn^{2+} + 2OH^{1-} \rightarrow Zn(OH)_2 \quad (5)$$

$$Zn(OH)_2 \rightarrow ZnO + H_2O \quad (6)$$

However, the electrochemistry related to iron ion/iron nitrate can be as follows:

$$Fe(NO_3)_2 + H_2O \rightarrow Fe^{3+} + NO_3^{1-} \quad (7)$$

$$Fe^{3+} + 3e^- \rightarrow Fe \quad (8)$$

$$Fe^{3+} + e^- \rightarrow Fe^{2+} \quad (9)$$

$$Fe^{2+} + 2e^- \rightarrow Fe \quad (10)$$

$$Fe^{3+} + 3OH^- \rightarrow Fe(OH)_3 \quad (11)$$

The mechanism for electro deposition of Fe_2O_3 is similar to that of ZnO, as mentioned above.

$$Fe(NO_3)_2 \rightarrow Fe_2O_3 + 3H_2O \quad (12)$$

4 Conclusions

Pure and Fe-ZnO thin films have been successfully synthesized on gold coated glass substrates by low-cost one-step electrodeposition technique at room temperature. The ZnO film presented a pure phase and a crystal size on the nano-metric scale. From X-ray diffraction analysis, the polycrystalline ZnO with wurtzite structure and the formation of Fe-ZnO composite was also confirmed. Also, the XRD analysis showed that the Fe ions replaced Zn atoms and incorporated into the crystal lattice positions of ZnO. The XRD pattern showed that the ZnO film suffers from a slight compressive stress for un-doped sample, which changes to tensile stress after Fe-doping and that the stress increases gradually with increasing Fe concentrations. The shift in the position of Raman E_2 high phonon mode downwards indicated that the ZnO films were subjected to increasing tensile stress with increase in Fe concentrations. The increased Fe concentration caused a distortion in the form of the crystals, suggesting the presence of tensile stress in ZnO films.

© 2017 NSP
Natural Sciences Publishing Cor.

References

[1] X. He, H. Yang, Z. Chen, S.S.Y. Liao, Physica B 407 (2012) 2895-2899.

[2] D. Fan, R. Zhang, X. Wang, Solid State Commun. 150 (2010) 824.

[3] S.H. Park, D. Ahn, Physica B 441 (2014) 12-16.

[4] H. I. Abdulgafour, F. K. Yam, Z. Hassan, K. Al-Heuseen and M. J. Jawad, J. Alloys Compd. 509 (2011) 5627.

[5] J. H. Choy, E. S. Jang, J. H. Jang and Y. W. Him, Adv. Mater.15 (2003) 1911.

[6] I. Novotny, P. Sutta, F. Mika and V. Trarozek, Proceedings of the International Conference on Microelectronics (IEEE Piscataway, N.J., 1995), p. 65.

[7] F. S. Mahnmood, R. D. Gould, A. K. Hassan and H. M. Salih, Thin Solid Films, 270 (1995) 376.

[8] P. Bonasewicz, W. Hirschwald and G. Neumann, Thin Solid Films 142 (1986) 77.

[9] A. Kuroyanagi, Jpn. J. Appl. Phys. 28 (1989) 219.

[10] H. Gpolaswamy, and P.J. Reddy, Semicond. Sci. Technol. 5 (1990) 980.

[11] H. Gomez, A. Maldonado, R. Asomoza, E. P. Zironi, J. Canetas-Ortega and J. Palacios-Gomez, Thin Solid Films, 293 (1992)117.

[12] T. Minami, H. Sato, H. Sohokara, S. Takata, T. Miyata and I. Fukuda, Thin Solid Films, 253 (1994)14.

[13] A. Ennaoui, M. Weber, R. Scheer, and H.J. Lewerenz, Sol.Energy Mater. Sol. Cells, 54 (1998) 277.

[14] Y. L. Liua, Y. C. Liua,b, Y. X. Liub, D. Z. Shena, Y. M. Lua, J. Y. Zhanga and X. W. Fana, Solid State Communications,138 (2006) 521.

[15] A.Y. Polyakov, A.V. Govorkov, N.B. Smirnov, N.V. Pashkova, S.J. Pearton, K. Ip, R.M. Frazier, C.R. Abernathy, D.P. Norton, J.M. Zavada, and R.G. Wilson, Mater. Sci. Semicond. Process., 7 (2004) 77.

[16] R. Janisch, P. Gopal, and N.A. Spaldin, J. Phys.: Condens. Matter, 17 (2005) R657.

[17] A. Debernardi, and M. Fanciulli, Appl. Phys. Lett., 90 (2007) 212510.

[18] K. Sato, and H. Katayama-Yoshida, Physica E, 10 (2001) 251.

[19] X.X. Wei, C. Song, K.W. Geng, F. Zeng, B. He, and F. Pan, J. Phys: Condens. Matter, 18 (2006) 7471.

[20] D. Karmakar, S.K.Mandal, R.M.Kadam, P.L. Paulose, A.K.Rajarajan, T.K.Nath, A.K.Das, I.Dasgupta, and G.P. Das, Phys. Rev. B, 75(2007) 144404.

[21] Q.J. Feng, D.Z.Shen, J.Y. Zhang, B.H.Li, Z.Z. Zhang, Y.M.Lu, and X.W.Fan., Mater. Chem. Phys., 112 (2008) 1106.

[22] Z.C. Chen, L.J. Zhug, X.M.Wu, Y.D. Meng, Thin Solid Films, 515 (2007) 5462.

[23] B. Panigrahy, M.Aslam, and D. J. Bahadur, Phys. Chem., C114 (2010) 11758.

[24] K.C.Barick, M.Aslam, V.P.Dravid, D.Bahadur. J Phys Chem C.,112 (2008)15163.

[25] J. Krüger, G.S. Sudhir, D. Corlatan, Y. Cho, Y. Kim, R.Klockenbrink, S. Rouvimov, Z. Liliental-Weber, C. Kisielowski, M. Rubin, and E.R.Weber Mater. Res. Symp. Proc. 482 (1998).

[26] R.R. Reeber, J. Appl. Phys. 41 (1970) 5063.

[27] Z.Z. Zhi, Y.C. Liu, B.S. Li, X.T. Zhang, Y.M. Lu, D.Z. Shen, X.W. Fan, J. Phys. D: Appl. Phys. 36 (2003) 719–722.

[28] X. H. Zhang, S. Y. Xie, Z. Y. Jiang, X. Zhang, Z.Q. Tian, Z.X. Xie, R.B. Huang and L.S. Zheng, J. Phys. Chem. B, 2003, 107(37) 10114-10118.

[29] J. H. Yang, J. H. Zheng, H. J. Zhai, and L. L. Yang, Cryst. Res. Technol. 44, No. 1, 87-91 (2009) / DOI 10.1002/crat.200800294.

[30] F. Decremps, J. Pellicer-Porres, A. M. Saitta, J. C. Chervin, and A. Polian, Phys. Rev. B 65, 92101 (2002).

[31] M. Scepanovic, M. Grujic-Brojcin, K. Vojisavljevic, S. Bernik, T. Sreckovic, J. Raman Spectrosc. (2009) 2546.

[32] S. Tripathy, S.J. Chua, M.S. Hao, E.K. Sia, A. Ramam, J. Zhang, W.H. Sun, L.S. Wang, J. Appl. Phys. 91 (2002) 584.

[33] A. Segura, J.A. Sans, F.J. Manjon, A. Munoz, M.J. Herrera-Cabrera, Appl. Phys. Lett. 83 (2003) 278.

[34] K.A. Alim, V.A. Fonoberov, A.A. Balandin, Appl. Phys. Lett. 86 (2005) 053103.

[35] H.Ishizaki, M. Imaizumi, S.Matsuda, M.Izaki, and T.Ito, Thin Solid Films, 411 (2002) 65.

[36] P. Hosik, A. Perla, A.D. Marc, M. Asok, C. Heechul, V.M. Nosang, Chem. Eng. J. 139 (2007) 208.

© 2017 NSP
Natural Sciences Publishing Cor.